JACS
JOURNAL OF THE AMERICAN CHEMICAL SOCIETY

Article

pubs.acs.org/JACS

Characterization of Photochemical Processes for H_2 Production by CdS Nanorod−[FeFe] Hydrogenase Complexes

Katherine A. Brown,[†] Molly B. Wilker,[‡] Marko Boehm,[†] Gordana Dukovic,*[,‡] and Paul W. King*[,†]

[†]Biosciences Center, National Renewable Energy Laboratory, Golden, Colorado 80401, United States

[‡]Department of Chemistry and Biochemistry, University of Colorado, Boulder, Colorado 80309, United States

Supporting Information

ABSTRACT: We have developed complexes of CdS nanorods capped with 3-mercaptopropionic acid (MPA) and *Clostridium acetobutylicum* [FeFe]-hydrogenase I (CaI) that photocatalyze reduction of H^+ to H_2 at a CaI turnover frequency of 380−900 s^{-1} and photon conversion efficiencies of up to 20% under illumination at 405 nm. In this paper, we focus on the compositional and mechanistic aspects of CdS:CaI complexes that control the photochemical conversion of solar energy into H_2. Self-assembly of CdS with CaI was driven by electrostatics, demonstrated as the inhibition of ferredoxin-mediated H_2 evolution by CaI. Production of H_2 by CdS:CaI was observed only under illumination and only in the presence of a sacrificial donor. We explored the effects of the CdS:CaI molar ratio, sacrificial donor concentration, and light intensity on photocatalytic H_2 production, which were interpreted on the basis of contributions to electron transfer, hole transfer, or rate of photon absorption, respectively. Each parameter was found to have pronounced effects on the CdS:CaI photocatalytic activity. Specifically, we found that under 405 nm light at an intensity equivalent to total AM 1.5 solar flux, H_2 production was limited by the rate of photon absorption (~1 ms^{-1}) and not by the turnover of CaI. Complexes were capable of H_2 production for up to 4 h with a total turnover number of 10^6 before photocatalytic activity was lost. This loss correlated with inactivation of CaI, resulting from the photo-oxidation of the CdS capping ligand MPA.

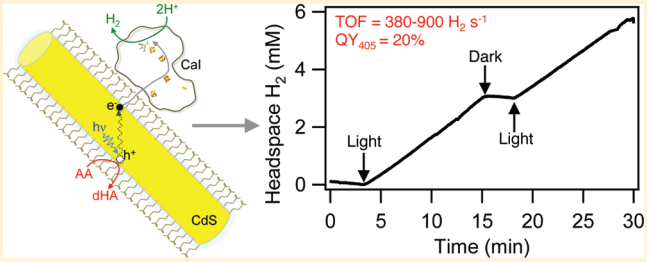

INTRODUCTION

The capture and conversion of solar energy to couple water oxidation to carbon fixation or hydrogen (H_2) production is an active area for developing renewable fuel technologies.[1−6] Studies of photosynthetic H_2 production,[7−12] first demonstrated in 1942,[13] have been models for inspiring the development of synthetic photochemical systems that are both more efficient and robust.[14] At the intersection of these two approaches, biohybrids integrate biological and synthetic molecules to engineer new photocatalytic assemblies for solar conversion. For example, photosystem I (PSI) has been assembled with inorganic H_2 production catalysts such as Pt nanoparticles[15−17] and transition metal compounds[18] or linked directly to H_2 activating enzymes, hydrogenases (H_2ases).[19,20] Complementary approaches have coupled H_2ases to particulate semiconductor materials[21−23] or onto conductive electrodes in photoelectrochemical devices.[24,25] In addition to these, there are many examples of completely synthetic photochemical systems,[26−29] including designs that couple semiconductors with inorganic surface catalysts.[30−33]

As H_2 activation catalysts, H_2ases exhibit some ideal characteristics including low activation energies, variation in bias, and a wide range of O_2 sensitivities, while utilizing organometallic catalytic sites composed of earth abundant metals.[34−40] Recently, single-molecule resolution electrochemistry experiments estimated the turnover frequency (TOF) of H_2 production by the [FeFe]-H_2ase from *Clostridium acetobutylicum* (CaI) at 21 000 s^{-1} at an overpotential of 150 mV.[41] This value for H_2 production TOF is among the highest for any H_2ase,[42,43] underscoring the potential of CaI as a model catalyst for developing biohybrids to investigate functional requirements for photocatalytic H_2 production.

We have shown that CaI forms catalytically active complexes with a variety of nanoparticles and functions as an electrocatalyst on nanostructured electrodes.[44,45] In particular, CaI forms photocatalytic complexes with 3-mercaptopropionic acid (MPA) capped CdTe nanocrystals.[21] These complexes displayed relatively short time scales of H_2 production and tended to decompose under illumination.[21] In the work described here, we have employed colloidal CdS nanorods to achieve greater photostability combined with a larger absorption cross-section and surface area. This material possesses excellent light-harvesting characteristics (molar absorptivities ~10^7 M^{-1} cm^{-1} at 405 nm, as described later in the text), and both bulk and nanoscale CdS have appropriate band-edge energies for water oxidation and proton reduction.[31,46−50] A number of photocatalytic systems derived from colloidal CdS nanorods attached to metallic catalysts have been reported to produce H_2 under solar irradiation.[30,31,49,51]

Received: December 13, 2011
Published: February 21, 2012

   dx.doi.org/10.1021/ja2116348 | *J. Am. Chem. Soc.* 2012, 134, 5627−5636

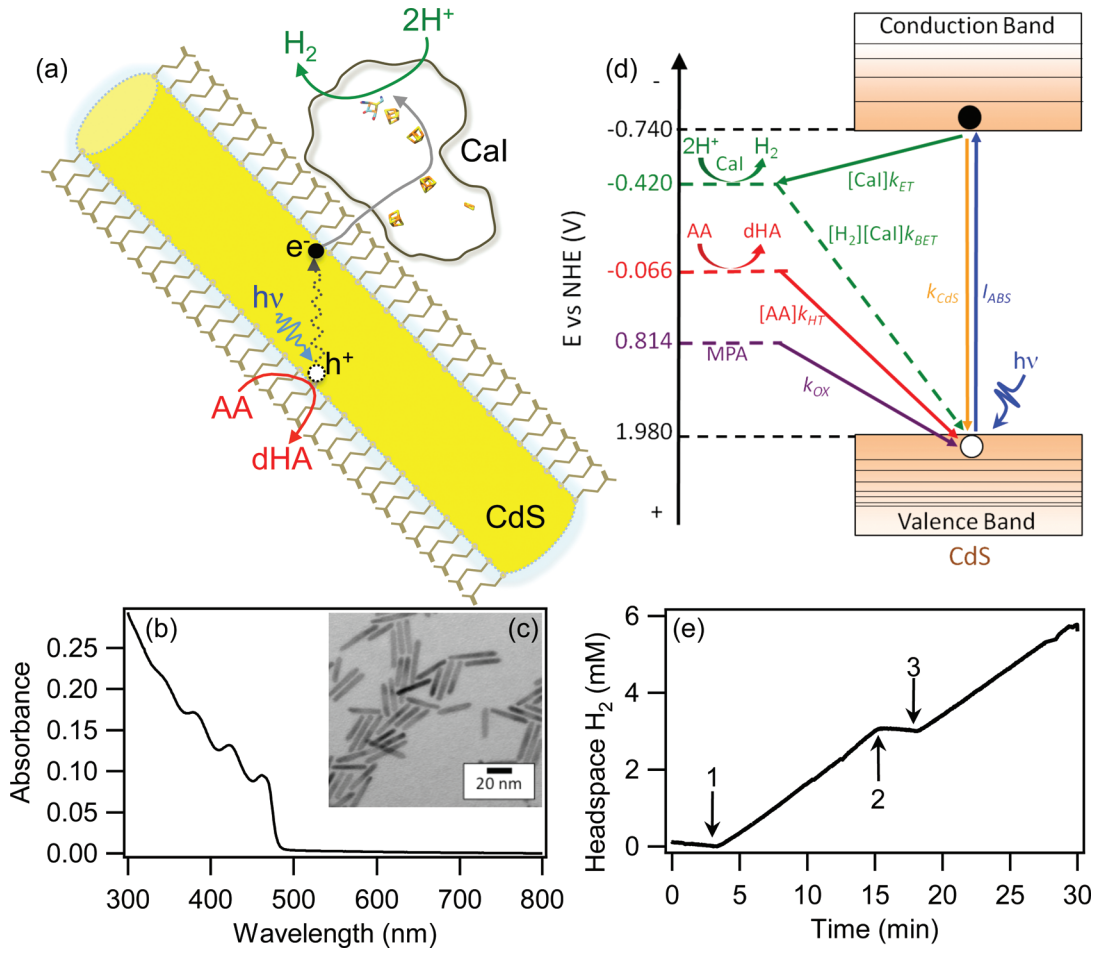

Figure 1. Properties of CdS nanorods and CdS:CaI complexes. (a) The proposed scheme for photocatalytic H_2 production by CdS:CaI complexes. Electron-transfer [FeS]-clusters and the catalytic H-cluster are shown in yellow (sulfur) and orange (iron). CdS and CaI are drawn to scale, while MPA molecules are enlarged ~5×. (b) UV−vis absorption spectrum of CdS nanorods in water. (c) TEM of typical CdS nanorods, average size 30 × 4.5 nm based on measurement of at least 200 nanorods. (d) Energy level diagram showing processes in photoexcited CdS that are relevant to H_2 production. (Abbreviations: AA, ascorbic acid; dHA, dehydroascorbate; CaI, [FeFe]-hydrogenase; E_g, band gap energy; k_{ET}, rate constant for ET from CdS to CaI; k_{HT}, rate constant for HT from CdS to AA; MPA, mercaptopropionic acid; k_{OX}, rate of photo-oxidation of surface-bound MPA ligands; k_{BET}, rate constant for ET from CaI to CdS (H_2 uptake); I_{ABS}, flux of absorbed photons; k_{CdS}, rate of excited state decay in CdS, including both radiative and nonradiative pathways (e.g., electron−hole recombination, carrier trapping). Potentials are shown vs NHE (pH 7, 1 atm H_2). (e) Photocatalytic H_2 production by CdS:CaI complexes in 50 mM Tris-HCl, 275 nM CdS, 360 nM CaI, and 100 mM AA illuminated with white light at 10 000 μE m^{-2} s^{-1}. Arrows show changes in illumination: (1) light on, (2) light off, (3) light on.

Furthermore, CdS nanocrystals can be functionalized with mercapto-carboxylic acids as capping ligands.[31,52] Such ligands promote adsorption of CaI on both quantum dots[21] and electrodes[41,53] and stabilize inorganic nanomaterials in aqueous buffers that are required for enzyme function.

Here we characterize the parameters controlling the photocatalytic H_2 production rates in biohybrid assemblies composed of [FeFe]-H_2ase CaI and MPA-capped CdS. The thermodynamics of self-assembly and the resulting orientations were investigated using kinetic analysis of CdS binding to CaI in competition with ferredoxin (Fd). We characterized the effect of CaI coverage in the context of CdS photon absorption and CaI catalytic flux. We also investigated the effects of hole-transfer and light intensity and found the H_2 production to be photon-limited under conditions approximating AM 1.5 solar flux. The quantum yield (QY) of the photocatalytic H_2 production was found to be ~20%. New insights on the instability observed for biohybrids under illumination, first observed for MPA−CdTe:CaI complexes,[21] are also provided. These analyses demonstrate how the contributions of individual processes govern photocatalytic activity and offer guidance in terms of the molecular design of future artificial photosynthetic systems.

MATERIALS AND METHODS

[FeFe]-hydrogenase Expression and Purification. The StrepII-tagged [FeFe]-H_2ase from *C. acetobutylicum* was expressed and purified from *Escherichia coli* as previously described.[54] Specific activities of CaI preparations were measured as the H_2 evolved from sodium dithionite (Riedel-de Haen) reduced methyl viologen (Sigma) (MV, 5 mM).[55] Purified CaI had specific activities of ~1300 μmol H_2 mg^{-1} min^{-1}, with protein concentrations determined by the Bradford assay using hemoglobin as the standard.[56]

Ferredoxin Expression and Purification. The mature form of the Fd protein PetF of *Chlamydomonas reinhardtii* was cloned and expressed in *E. coli* as described in the Supporting Information.

Synthesis of CdS Nanorods. The synthesis was adapted from previously published procedures (Supporting Information).[57,58] Synthesis and processing were conducted under an inert argon atmosphere at ~620 Torr (atmospheric pressure in Boulder, CO). The resulting solutions consisted of nanorods with average diameter of

dx.doi.org/10.1021/ja2116348 | J. Am. Chem. Soc. 2012, 134, 5627−5636

4.5 nm and average length of 30 nm. Molar absorptivity (ε) for CdS nanorods was determined by correlating absorption spectra with Cd^{2+} concentrations determined by elemental analysis (ICP-OES) of acid-digested samples. The value of ε was estimated to be 1710 M^{-1} cm^{-1} per Cd^{2+} at 350 nm. The number of Cd^{2+} per nanorod was estimated from average length and diameter measurements determined from TEM images.

Ligand Exchange on CdS Surface. The ligand exchange procedure was adapted from Amirav et al.[31] First, 1.27 mmol of 3-mercaptopropionic acid (3-MPA, Sigma Aldrich ≥99%) was dissolved in 20 mL of methanol. The solution pH was increased to 11 with tetramethylammonium hydroxidepentahydrate salt (Sigma Aldrich). A sample of nanocrystals was precipitated from toluene solution using methanol. The precipitated nanocrystals were then mixed with the MPA/methanol solution until the mixture was no longer cloudy. The water-soluble nanocrystals were precipitated with toluene. The resulting particles were dried under vacuum and redispersed in Tris buffer, pH 7.

Transmission Electron Microscopy. TEM samples were prepared by drop casting on carbon film, 300 mesh copper grids from Electron Microscopy Sciences. Images were taken on a 100 KV Phillips CM100 transmission electron microscope equipped with a bottom-mounted 4 megapixel AMT v600 digital camera. Lengths and diameters were determined from an average of at least 200 particles.

Determination of Reduction Potential of CdS Nanorods. Mixtures of 83 nM CdS nanorods and 167 nM MV (Sigma) were combined under an anaerobic Ar atmosphere in buffers of varying pH (2, 2.5, 3, 3.4, 4, and 4.5).[59,60] Samples were illuminated for 10 min with 405 nm LED light at 800 μE m^{-2} s^{-1} intensity. Absorbance spectra were collected on a Beckman DU800 and the concentration of reduced MV was determined by absorbance at 606 nm (A_{606}) (Supporting Information). The potential of the conduction band electrons in photoexcited CdS at standard reaction conditions was determined by extrapolation to pH 7 using the Nernst equation.

Assembly of CdS:CaI Complexes. Mixtures of CdS nanorod and CaI solutions for all experiments were prepared in buffer (50 mM Tris-HCl, 5 mM NaCl, 5% glycerol, pH 7), under an anaerobic atmosphere of 4% H_2/96% N_2, and then sparged with 100% Ar. The CdS concentration was determined from absorbance at 350 nm (ε = 9 × 10^6 M^{-1} cm^{-1}). Samples were stirred for at least 10 min to ensure complete assembly prior to all experiments (see Figure S2, Supporting Information).

Ferredoxin–CdS Competition Kinetics. Mixtures of CdS nanorods and CaI in molar ratios of 0:1, 2:1, 5:1, and 10:1 CdS:CaI were prepared under an anaerobic atmosphere of 4% H_2/96% N_2 and then sparged with 100% Ar, with a fixed CaI concentration of 28 nM for all samples. Stock Fd solutions were reduced with 5 mM sodium dithionite and added to CdS:CaI mixtures to achieve the desired Fd concentration (0, 15, 30, 60, 150, 300 μM). The headspace H_2 was measured after 6 min by injection into an Agilent 7890A gas chromatograph fitted with a 5 Å molecular sieve column (Supelco). A constant low level of background H_2 production from reduction of CaI by 5 mM sodium dithionite was observed in all reactions and was subtracted from the sample containing Fd.

Light-Driven H_2 Production. Samples of CdS:CaI were prepared as above. Solutions contained 100 mM ascorbic acid (AA, Fluka) unless otherwise noted. Gas analysis of sample headspace confirmed H_2 removal. Samples were illuminated for 10 min with an Ocean Optics 405 nm LED light source (750 mW, 500 mA) at 800 μE m^{-2} s^{-1} (light meter LI-250, LI-COR Biosciences) unless otherwise noted. The photon flux of AM 1.5 photons with sufficient energy to excite CdS nanorods (E_g = 464 nm) was calculated to be 450 μE m^{-2} s^{-1}. Samples were incubated in 1.5 mL serum vials with an illuminated surface area of 5 mm^2 unless otherwise noted. Light intensities were confirmed before each illumination experiment. Headspace H_2 was measured at 10 min by GC injection or in real-time by continuous measurement by an Omnistar capillary mass spectrometer (Pfeiffer). Turnover frequencies (TOF) for photochemical H_2 production are expressed in units of mol H_2 (mol CaI)$^{-1}$ s^{-1}.

Quantum Yield Measurements. Mixtures of CdS nanorods and CaI in molar ratios of 1:0.67 CdS:CaI (14 nM CdS, 9 nM CaI) were prepared as above in buffer with 100 mM AA. Samples were illuminated in a quartz cuvette with a 3 × 5 mm window with a 1 mW 405 nm laser pointer (Laserglow Technologies) with a spot size of 6 mm^2. Light intensity passing through the sample was measured using a Newport model 1918-R power meter with an 818-ST-UV UV-enhanced silicon photodetector. The difference between light intensity transmitted through a control cuvette containing 50 mM Tris-HCl buffer (pH 7) and through the sample cuvette corresponded to absorbed intensity. The amount of H_2 produced was measured after 10 min of illumination by GC. The quantum yield was defined as QY = (mol H_2 produced/mol photons absorbed) × (2 mol photons/mol H_2).

RESULTS AND DISCUSSION

Assembly and Orientation of Photocatalytically Active CdS:CaI Complexes. Figure 1a shows a structural model of the complex formed between CaI and MPA-capped CdS nanorods (referred to here as CdS), with a predicted conformation based on the surface charges of the two components. The MPA bonds to the CdS surface via the thiol group, with the solvent-exposed carboxylate group imparting a negative surface charge at pH 7. As previously shown, MPA-capped nanoparticles formed complex with CaI via electrostatic interactions and were predicted to orient the positively charged enzyme surface near the distal [4Fe–4S] cluster toward the MPA carboxylate group.[21,61] In a similar fashion, the CdS used here was expected to bind to this site on CaI, which is also the site for ferredoxin (Fd) interaction during ET in vivo.[55,62] When CdS and CaI were mixed, complexes self-assembled and reached full photocatalytic activity within 10 min (Figure S2, Supporting Information). The H_2 production rates were linear under illumination with white light in the presence of 100 mM AA, and no significant H_2 production was seen when the illumination is turned off (Figure 1e) or when any of the components (CdS, AA, or H_2ase) were absent.

To confirm the predicted conformation model of the CdS:CaI binding complex, the effect of CdS on Fd-driven H_2 production by CaI was tested (Figure 2). The analysis of the inhibition kinetics by Dixon plot[63,64] (Figure 2a) or double-reciprocal plot[65] (Figure 2b) was consistent with a linear mixed-type inhibition, as described by the equilibrium model shown in Figure 2c. The values for K_I, the dissociation constant for inhibitor (CdS) and CaI binding, and α, the factor by which K_S changes in the presence of CdS, are shown in Table 1. A key feature of mixed inhibition is the ability of the EI complex (CdS:CaI) to bind the substrate, reduced Fd, in a nonactive complex, ESI. Thus, as CdS concentration increases, the soluble Fd pool is effectively decreased, giving rise to the measured value of α. For CdS:CaI, this behavior is likely explained by binding of the Fd to the CdS nanorod. Although the Fd surface that binds to CaI is negatively charged, the opposing face is more positively charged, forming a dipole.[66] Thus, Fd could bind to the negatively charged MPA–CdS via an electrostatic interaction, as has been shown in the case of MPA-modified Au surfaces.[67] On the basis of the K_I value, binding of CdS to CaI is stronger than that of Fd, possibly due to a larger contact surface between CdS and CaI and stronger electrostatic interaction. On the other hand, the Fd–CaI ET complex by necessity is exchangeable to allow for multiple reduction–oxidation reactions between Fd and other donor/acceptor molecules in the cell. By creating a stable CaI–CdS interaction, ET is no longer diffusion limited, and turnover rates of CaI

dx.doi.org/10.1021/ja2116348 | J. Am. Chem. Soc. 2012, 134, 5627–5636

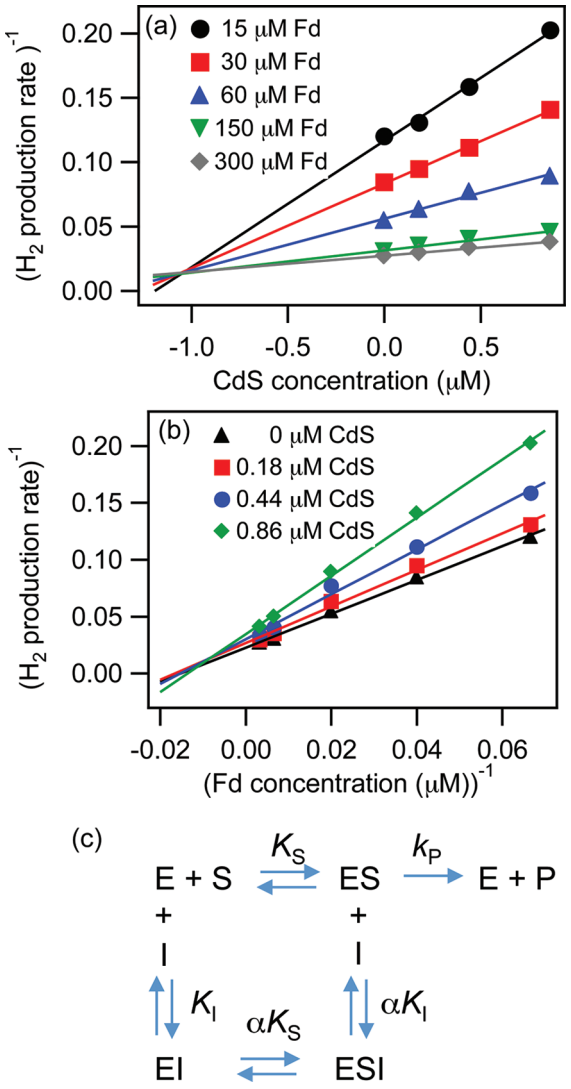

Figure 2. Kinetics of CdS inhibition of Fd-mediated CaI H_2 evolution in the dark. The CaI concentration was fixed at 28 nM, and the CdS concentration was varied between 0 and 1.1 μM to achieve molar ratios of 0:1, 1.5:1, 3.8:1, and 7.5:1 CdS:CaI. Reduced Fd (in 2.5 mM sodium dithionite) was added to yield final concentrations of 15, 30, 60, 150, and 300 μM. The total production of H_2 was measured after 6 min in the dark. The measured K_M (K_S in the equation) of CaI for Fd in the absence of CdS was found to be 44 μM. (a) Dixon plot of the inverse of H_2 production TOF (mol^{-1} H_2 mol CaI s) versus CdS concentration (μM). The measured K_I of CdS is ~1.4 μM (average of the values shown in Table 1). (b) A double-reciprocal plot of inverse H_2 production rate versus inverse Fd concentration. (c) Equilibrium model of linear mixed-type inhibition, where E is CaI, I is CdS, S is Fd, and P is H_2.

Table 1. Inhibition Constants for CdS on Fd-Mediated H_2 Evolution by CaI

analysis method[a]	kinetic constants
Dixon plot, $[CdS]$ vs $(TOF)^{-1}$	K_I = 1.28 ± 0.19 μM
	α = 2.77 ± 0.58
double reciprocal, $[Fd]^{-1}$ vs $(TOF)^{-1}$	K_I = 1.58 ± 0.26 μM
	α = 2.31 ± 0.38

[a]TOF = mol H_2 $(mol\ CaI)^{-1}$ s^{-1}.

might approach those measured using electrochemical techniques.

Determination of the CdS Band-Edge Reduction and Oxidation Potentials. The band structure of CdS and the formal potentials of the charge carrier acceptors are shown in Figure 1d. The conduction band (photoexcited electron) potential in CdS was measured in solution by photoreduction of the redox-active dye methyl viologen (MV^{2+}), for a range of pH values (Figure S1, Supporting Information).[59,60] The valence band (hole) potential was calculated by subtracting the CdS optical band gap energy (464 nm, 2.9 eV, Figure 1b) from the measured potential of the conduction band. The CaI operating potential is estimated by the Nernst equation of the H^+/H_2 redox couple (pH 7, 1 atm H_2).[55] The overpotential of the CdS conduction band is therefore ~320 mV (vs NHE). Also shown is the electrochemical potential of the ascorbic acid (AA)−dehydroascorbate (dHA) redox couple,[68] which is used here as the sacrificial electron donor to regenerate the CdS ground state.

Effect of the CaI:CdS Ratio on Photocatalytic Rates. The scheme shown in Figure 1d illustrates the photochemical processes that contribute to H_2 production activity of CdS:CaI complexes. Photon absorption by CdS (I_{ABS}) results in the generation of electron−hole pairs. These are coupled to catalysis through the transfer of conduction band electrons to CaI at a rate that is proportional to the product of $[CaI]k_{ET}$ (referred to as "ET"), and hole scavenging by oxidation of AA at a rate proportional to $[AA]k_{HT}$ (referred to as "HT"). These external processes compete with oxidation of the MPA ligands (k_{OX})[31,69] and internal recombination pathways in CdS (k_{CdS}). The individual contributions of I_{ABS}, ET, and HT can be manipulated by changes in light intensities, the stoichiometric distribution of molecular complexes, and AA concentration, respectively. Adjusting the relative contribution of each process allows for a more complete understanding of how photon energy is allocated and how each process affects the overall conversion efficiency.

The first parameter tested was the ET rate, which was varied by changing the molar ratio of CaI molecules per CdS nanorod (rate of ET ∝ $[CaI]k_{ET}$) and measuring the photocatalytic H_2 production rates (Figure 3). The light intensity and the concentrations of AA and CdS were fixed to ensure that the rates of photon absorption (I_{ABS}), HT (∝$[AA]k_{HT}$), and the

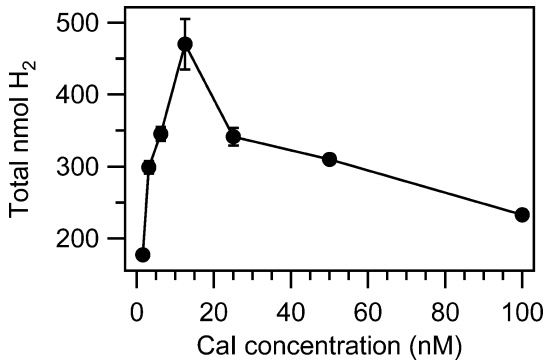

Figure 3. Effect of complex molar ratio of photocatalytic H_2 production by CdS:CaI. Mixtures prepared with a fixed CdS concentration of 19 nM and CaI concentrations between 1.58 and 100 nM to give molar ratios of 1:5, 1:2.5, 1:1.33, 1:0.67, 1:0.33, 1:0.167, and 1:0.083 CdS:CaI solutions. Samples were illuminated for 10 min with a 405 nm LED at 800 μE m^{-2} s^{-1}.

dx.doi.org/10.1021/ja2116348 | J. Am. Chem. Soc. 2012, 134, 5627−5636

number of available photogenerated electrons were constant across all samples. A 405 nm light intensity of 800 μE m^{-2} s^{-1} was used to approximate the flux AM 1.5 photons absorbed by CdS. We observed that H_2 production rates initially increased with increasing CaI concentration up to 12.5 nM CaI (molar ratio 1:0.67 CdS:CaI) but then declined at higher CaI concentrations. We had expected that as CaI concentration increased the level of H_2 production would also increase, since the fraction of the photoexcited electrons decaying by ET, rather than internal recombination in CdS, should increase with CaI concentration. We hypothesize that the decline in rate at high CaI coverage is due to back electron transfer (BET) arising from (i) CaI oxidation of H_2 (Figure 1d, k_{BET}) and/or (ii) competition for electrons among multiple CaI molecules. Both effects would reduce the H_2 production TOF and total H_2 levels in samples with high CaI:CdS ratios and multiple CaI molecules per CdS.

Statistical Analysis of CdS:CaI Molar Ratio. If the hypothesis above is valid, we would expect that complexes composed of a single CaI bound to a single CdS would exhibit peak H_2 production efficiencies that decrease as multiple CaI molecules bind to each CdS. Thus, the amount of H_2 generated by a solution of CdS:CaI complexes would scale with the relative concentration of the 1:1 fraction.

To test this model, a statistical analysis of the molecular compositions of each ratio was compared to the photocatalytic H_2 production rates and TOF. Since the surface area of CdS nanorods (~456 nm^2) is significantly larger (~26 times) than the binding surface of CaI (17.5 nm^2),[61] each nanorod should be able to accommodate several molecules of CaI (5−10) before steric effects limit additional binding. Thus, the probability of CaI binding to CdS was assumed to be independent of whether another CaI was present (up to the limit of 10 CaI molecules per CdS), and the fractional population of each ratio was modeled using a Poisson distribution.

As shown in Figure 4a, the distribution of 1:1 and 2:1 CdS:CaI complexes (complete distributions for each molar ratio are listed in Table S1, Supporting Information) changes as a function of CaI concentration. Using the analysis performed in Figure 4a, the concentration of 1:1 complexes for each ratio was plotted versus the total H_2 produced. A linear fit of the plot (Figure 4b) shows that as the fractional level of 1:1 increased, rates also increased. Furthermore, a plot of the 1:1 fraction (of all *occupied* nanorods) against the CaI TOF for each ratio predicts that a maximal TOF value of 412 s^{-1} (under 405 nm light at 800 μE m^{-2} s^{-1}) should be observed for a 100% solution of 1:1 complexes. Together the data presented in Figure 4 show that the 1:1 complexes, under these conditions, make the most efficient use of CaI to achieve the highest TOF values and H_2 production rates.

Contribution of AA and HT to CdS:CaI Photocatalytic Rates. In order to investigate the effect of the contribution of HT, we examined the effect of AA concentration on photocatalytic H_2 production by a CdS:CaI (1:0.67 CdS:CaI molar ratio) under two different intensities of 405 nm light (Figure 5a). In this case, the contribution of HT is changing, but the photon flux, complex concentrations, and ratio distributions are fixed. Under both light intensities, the TOF of the complexes increased to maximal values as the AA concentrations increased. At 800 μE m^{-2} s^{-1} (black circles) the TOF for H_2 production began to saturate at ~10 mM AA and at ~25 mM AA under illumination at 2000 μE m^{-2} s^{-1} (red squares). Thus, a range of 10−25 mM AA was required to achieve maximal photocatalytic rates. Michaelis−Menten kinetic analysis of the data presented in Figure 5a showed that the AA interaction with CdS has an average k_{cat}/K_m of 10^4

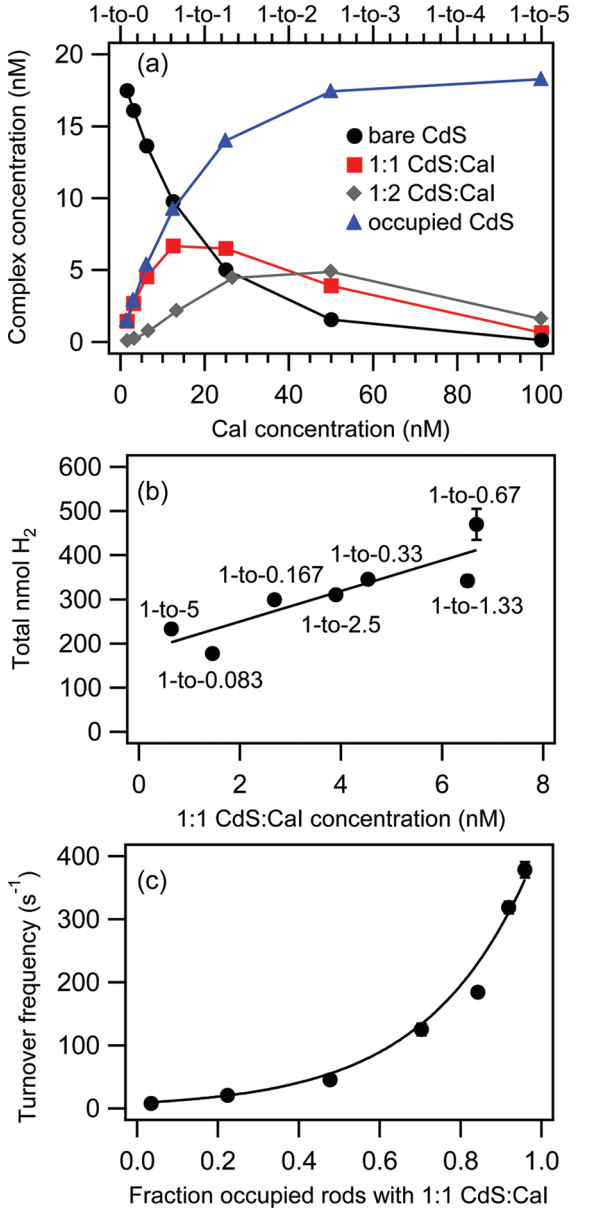

Figure 4. Statistical analysis of photocatalytic H_2 production by CdS:CaI complexes. (a) Concentrations of specific molecular complexes within each solution of CdS:CaI. Concentrations are calculated using the Poisson distribution to determine the fraction of 19 nM CdS with a specific CaI coverage for the molar ratios of 1:5 (100 nM CaI), 1:2.5 (50 nM CaI), 1:1.33 (25 nM CaI), 1:0.67 (12.5 nM CaI), 1:0.33 (6.25 nM CaI), 1:0.167 (3.13 nM CaI), and 1:0.083 (1.56 nM CaI) CdS:CaI. Bare CdS (black circles) has no CaI adsorbed, 1:1 CdS:CaI (red squares) has one CaI absorbed per CdS, 2:1 CdS:CaI (gray diamonds) has 2 CaI adsorbed per CdS, and total occupied CdS (blue triangles) is the sum of all CdS with ≥1 CaI adsorbed per CdS. (b) total nanomoles of H_2 produced under 10 min illumination with a 405 nm LED at 800 μE m^{-2} s^{-1} vs the concentration of 1:1 CdS:CaI calculated from the Poisson distribution for each CaI concentration. The solid trace is a linear fit. (c) CaI TOF [mol H_2 (mol CaI)$^{-1}$ s^{-1}] vs the fraction of occupied nanorods that are 1:1 complexes, calculated from the Poisson distribution. The line is an exponential fit to $y = Ae^{bx}$ (A = 7.17, b = 4.05).

dx.doi.org/10.1021/ja2116348 | J. Am. Chem. Soc. 2012, 134, 5627−5636

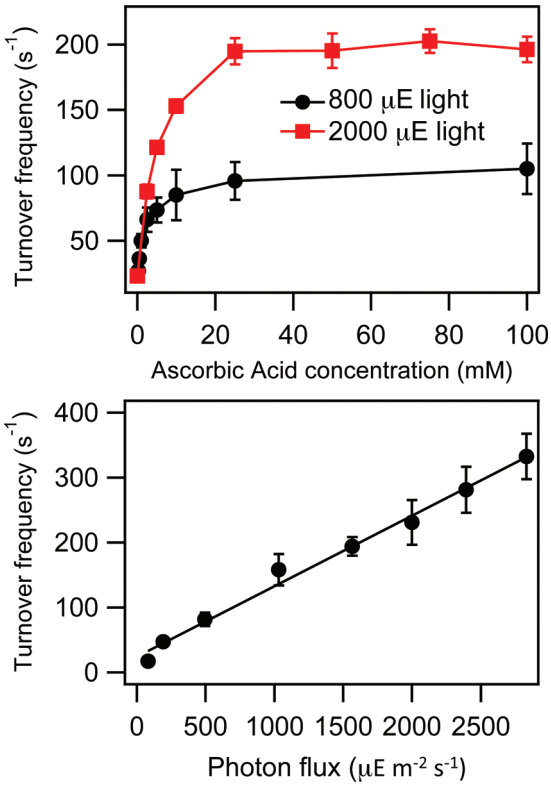

Figure 5. Effects of hole scavenger and light intensity on photocatalytic H_2 production by CdS:CaI complexes. (a) Effect of AA concentration on TOF of H_2 production [mol H_2 (mol CaI)$^{-1}$ s^{-1}] by a 1:0.67 mixture of CdS:CaI. The sample concentrations were fixed at 14 nM CdS and 9 nM CaI. Samples were illuminated for 10 min with 405 nm light at 800 (black circles) or 2000 (red squares) μE m^{-2} s^{-1}. (b) Effect of light intensity on TOF of H_2 production [mol H_2 (mol CaI)$^{-1}$ s^{-1}] by 1:0.67 CdS:CaI solutions. The sample concentrations were fixed at 14 nM CdS and 9 nM CaI, with 100 mM AA as the hole-scavenger. Each sample was prepared in a cuvette with a 3 × 5 mm window and illuminated with a 405 nm light source for 10 min at the designated intensity. Also shown is a linear fit (slope = 0.108 μE m^{-2}; y intercept = 24.5 s^{-1}).

s^{-1} M^{-1} during H_2 production (Table S3, Supporting Information), which is ~10^6 below the upper limit for diffusion-limited processes.[70,71] Moreover, although ~2200 AA (0.2 nm^2) can bind per CdS, it must actively exchange during turnover to maintain charge balance in CdS. Binding constants of AA for cysteine capped CdS quantum dots have been measured at 1 mM,[72] consistent with the 1−5 mM K_m values we measured here (Figure 5a and Table S3, Supporting Information). Thus, AA is required at greater than millimolar levels to maintain the fast TOF of the CdS:CaI complexes during photochemical H_2 production due to the weak, diffusion-limited reaction kinetics with the CdS.

Quantum Yield of H_2 Production. The QY of photocatalytic H_2 generation by the 1:0.67 CdS:CaI solution was measured using a 405 nm laser (Table S2, Supporting Information). This laser light source produces a collimated beam with a photon flux of 540 μE m^{-2} s^{-1}. Measurement of photons absorbed (~16% of total) and H_2 produced showed that the QY of CdS:CaI was 20.4 ± 1.9% based on two photons (one photon = one electron) per H_2. This compares favorably to the photosynthetic efficiencies of microalgae.[14,73] It should be noted that this QY value is an average value for the distribution of molecular complexes present in the 1:0.67 ratio. This will include a high fraction (~51%) of bare CdS, which is photocatalytically silent, and some with multiple (>1) CaI molecule coverage, which contribute to a decrease in H_2 production. Thus, it is likely that QY will vary with CdS:CaI molar ratio and that a solution consisting entirely of 1:1 coverage CdS:CaI would yield a higher QY value.

Effect of Light Intensity on CdS:CaI Photocatalytic Rates. A critical question in the design of biohybrid photocatalytic systems is whether the overall yield is limited by light absorption or the rate of catalysis (TOF). Recent measurements of CaI TOF on MPA−Au electrodes[41] can be used to estimate that for an overpotential of 320 mV, as is the case with CdS nanorods, the expected TOF would be ~4000 s^{-1}. Since this value was not observed under the illumination conditions used here, H_2 production might be limited by the availability of photogenerated electrons. If this were the case, the H_2 production levels would be expected to increase with higher light intensities as the rate of the ET process approaches the maximum TOF of CaI.

Figure 5b shows that the H_2 generation rate scales linearly with light intensity (for the CdS:CaI ratio of 1:0.67). This indicates that the QY of H_2 production is constant over the intensity range examined and suggests that the rate at which the enzyme is able to convert the photoexcited electrons into H_2 is higher than the rate at which the electrons are supplied. At a photon flux of 540 μE m^{-2} s^{-1}, we estimate that each nanorod is excited on average 1000 times s^{-1} (ε = 6.5 × 10^6 M^{-1} cm^{-1}). At a H_2 production QY of 20%, this corresponds to an enzyme TOF of 100 s^{-1}.

Using the linear fit of TOF vs light intensity in Figure 5b, the light intensity value for which electron flow (excitation rate × quantum efficiency of ET) will match CaI turnover for a 100% solution of 1:1 complexes can be estimated. Assuming that the response remains linear, the CaI TOF value of 4000 s^{-1} will be reached at 405 nm light intensity of ~11 000 μE m^{-2} s^{-1}. This is ~25-fold higher than the integrated flux of AM 1.5 photons that can be used by CdS (450 μE m^{-2} s^{-1}, with λ < 464 nm) but similar in magnitude to full-spectral AM 1.5 flux of ~7000 μE m^{-2} s^{-1}. Thus, H_2 production in CdS:CaI complexes is photon-limited due to the absorption range of CdS, and efficiencies under solar illumination can be improved by widening the range of light-absorption, so that catalytic rates can be matched at solar flux, and by improving electron transfer efficiencies.

Long-Term Behavior of CdS:CaI Complexes. The long-term photocatalytic H_2 production by CdS:CaI is shown in Figure 6a. The sample consisted of a 1:0.67 mixture of CdS:CaI in 100 mM AA that was illuminated continuously for 6 h. The UV−vis spectra of the reactions during the 6 h period showed that AA oxidation (monitored as changes in absorbance at 360 nm)[74,75] occurred only in the presence of CaI (Figure S4, part a vs d, Supporting Information). The peak rate of H_2 production occurred within the first 30 min of illumination, followed by a slow, continuous decline in the observed rate throughout the next several hours. As a result, after 4 h of continuous illumination, there was little or no further accumulation of H_2. The total turnover number (TON) for CdS:CaI was approximately 1 million. We tested several hypotheses to explain the noticeable decline in H_2 production rate after 4 h. (i) Since reactions are sealed, elevated H_2 levels lead to increased H_2 partial pressure for H_2 oxidation by CaI.[55] However, replacement of the headspace gas with 100% Ar every 10 min during illumination did not alter the long-term decline

dx.doi.org/10.1021/ja2116348 | J. Am. Chem. Soc. 2012, 134, 5627−5636

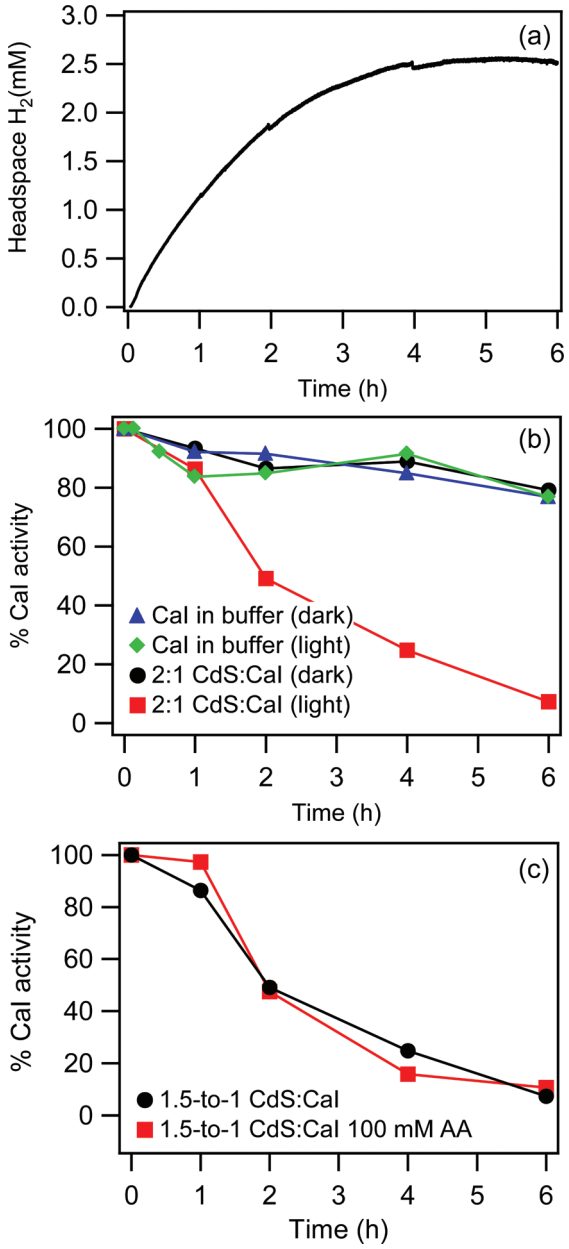

Figure 6. Effects of long-term illumination of 1:0.67 CdS:CaI solution. (a) Photocatalytic H_2 production by a 1:0.67 CdS:CaI solution, 14 nM CdS, 9 nM CaI, 100 mM AA, illuminated 6 h with 800 μE m^{-2} s^{-1} of 405 nm LED light. (b) Effect of illumination on CaI activity in CdS:CaI complexes. A concentration of 9 nM CaI in 50 mM Tris-HCl stirred for the appropriate time alone in the dark (blue triangle) or illuminated with 800 μE m^{-2} s^{-1} of 405 nm LED light (green diamonds); mixture of 14 nM CdS, 9 nM CaI in 50 mM Tris-HCl stirred in the dark (black circles) or illuminated with 800 μE m^{-2} s^{-1} of 405 nm LED light (red squares). CaI activity in all samples was measured in 5 mM MV at the specified time. (c) Effect of 100 mM AA on CaI long-term activity. A mixture of 14 nM CdS and 9 nM CaI in 50 mM Tris-HCl stirred under illumination with 800 μE m^{-2} s^{-1} of 405 nm LED light with (red squares) and without (black circles) 100 mM AA.

in steady-state H_2 production rates (Figure S4, Supporting Information). (ii) Although the oxidation of AA was evident during H_2 production (time points 0–4 h, Figure S4a, Supporting Information), based on the net H_2 produced the residual [AA] remained well above the level needed to support maximal rates (20 mM at 800 μE m^{-2} s^{-1}, Figure 5a) and was not the limiting component. (iii) We also ruled out precipitation and degradation of the CdS nanorods. There was no evidence of significant changes in the UV–vis absorbance profile or in the dimensions based on TEM images (Figures S4 and S5, Supporting Information). Thus, none of these factors could account for the decline in photocatalytic rates shown in Figure 6a.

To test whether there was a direct effect on the catalytic capacity of CaI during long-term photocatalysis, the activity of CaI was monitored using the MV-dependent H_2 evolution assay. As shown in Figure 6b CaI alone showed no evidence of light-dependent inactivation (Figure 6b, green plot) compared to the enzyme kept in the dark (Figure 6b, blue plot), and both the light and dark incubated samples lost the same ~20% of activity during the 6 h period. When in a complex with CdS, CaI showed a similar level of stability as the free enzyme if incubated in the dark. However, when CdS:CaI complexes were illuminated, the CaI was clearly inactivated (Figure 6b, red plot). Notably, the inactivation kinetics closely followed the decline in H_2 production rate (Figure 6, part a vs b), with an acceleration in rate after 1 h. At the 4 h period, a small but significant (~20%) fraction of active CaI remained even after the photocatalytic rates had approached zero. Thus, the loss of catalytically active CaI results from a light-dependent process occurring within the MPA–CdS, but does not completely account for the loss in photocatalytic H_2 production by CdS:CaI.

It has been shown that long-term illumination of ligand-capped Cd chalcogenide nanocrystals results in the loss of surface thiol ligands.[52,69,76] On the basis of the effects of similar sulfur compounds on the activities of other metalloenzymes, we hypothesize that this process in MPA–CdS results in release of free MPA that in turn inhibits CaI activity.[77−79] To test this, the effect of MPA on CaI H_2 evolution activity was measured over time (Table 2). MPA led to inactivation of CaI in a time-dependent manner, with nanomolar concentrations effectively reproducing the loss in CaI activity in CdS:CaI complexes. This amount of MPA is ~0.2% of the MPA coverage on CdS nanorods, so deactivation of CaI occurred before MPA oxidation was sufficient to contribute to precipitation of CdS. We also tested the effect of Cd^{2+} on CaI activity and found no effect at 760 nM Cd^{2+} (Figure S6, Supporting Information), which is equivalent to the MPA concentration that led to maximal inactivation rates of CaI (Table 2). Together the data support the hypothesis that prolonged illumination of the CdS:CaI results in the slow light-driven loss of MPA from the nanorod surface, which in turn leads to the progressive loss of CaI activity. The mechanism of CaI inactivation by MPA is not yet clear and may arise from active site inhibition,[79] extraction

Table 2. Effect of [MPA] on CaI Inactivation

[MPA] (nM)	MPA:CaI molar ratio[a]	I_{50} (h)[b]
19	0.5	6
38	1	4
76	2	3
190	5	2
380	10	0.75
760	20	>0.1

[a]38 nM CaI. [b]The CaI activity was measured as H_2 evolution using sodium dithionite reduced MV (5 mM)

dx.doi.org/10.1021/ja2116348 | J. Am. Chem. Soc. 2012, 134, 5627–5636

of the distal iron−sulfur clusters,[77,80] or a combination of both. Interestingly, the loss of CaI activity does not appear to be affected by the presence of AA (Figure 6c). Thus, if the free form of MPA accumulates through oxidation by photoexcited holes, this process is competitive with, or may be dominant over, hole-scavenging by AA. Moreover, as MPA molecules are lost from the CdS surface, the resulting defect sites may act as electron sinks. In combination, these effects would explain the lack of photocatalytic production of H_2 in the absence of AA.

CONCLUSIONS

In this study, we present an analysis of the photocatalytic behavior of CdS:CaI complexes. The QY for H_2 production was 20%, with TOF values [mol H_2 (mol CaI)$^{-1}$ s^{-1}] of up to 380 under 405 nm light and 983 under high intensity (30 000 μE m^{-2} s^{-1}) white light (Table S3, Supporting Information), significantly higher than the current values for PSI hybrid systems.[16,18,20,81] The high TOF was a result of directed assembly, in which site-specific binding of the MPA−CdS to a positive patch on the CaI surface facilitates rapid ET from CdS to the CaI electron transport chain iron−sulfur clusters. This molecular orientation was confirmed by competition assays, where CdS acted as an inhibitor of Fd-driven H_2 production by CaI. The activity of complexes was manipulated by changing the contributions of the individual photocatalytic processes. The CdS:CaI molar ratios controlled the contribution of productive ET, with the 1:1 coverage CdS:CaI complexes having the highest TOF. Overall H_2 production rates are reduced by the mismatch of excitation rate and enzyme TOF at solar-flux levels, which we hypothesize contributes to BET from CaI to CdS (as a form of hole-scavenging). The concentration of AA was shown to control the contribution of external HT in regeneration of the CdS ground state. Long-term stability was affected by photodegradation of the MPA−CdS, limiting the TON to a value of 10^6 H_2 before cessation of photocatalysis. The photodegradation was at least in part due to the oxidative loss of MPA from the CdS surface (Figure 1d), which could be improved through stabilizing surface ligands or enhancing the HT reaction to limit ligand photo-oxidation. Long-term efficiencies in other photocatalytic systems also suffer from photodegradation of the light-absorbing components, but due to different processes. For example, the instability of CdTe:CaI biohybrids observed previously might be due to energetic mismatch of the CdTe valence band and MPA oxidation potentials (in contrast to CdS as shown in Figure 1d) resulting in photodegradation of the CdTe. In dye-sensitized Ru(bpy)−TiO_2−[NiFeSe]-H_2ase complexes,[22,23] photocatalytic activity was lost due to photodegradation of the Ru(bpy)−TiO_2 and not to any loss in H_2ase activity. ZnSe/CdS−Pt complexes also lose activity but are reactivated by addition of fresh mercapto-carboxylic acid ligands.[30]

The light absorption of semiconductor nanocrystals is robust and saturates at very high light intensities (≫E m^{-2} s^{-1}).[82] Photosynthesis, on the other hand, saturates at ∼400 μE m^{-2} s^{-1} (measured as the O_2 evolution rate) or ∼16% of the peak photosynthetic active radiation (PAR) solar flux of 2500 μE m^{-2} s^{-1}.[83] Saturation arises from several factors, including catalysis and intermolecular ET rates that are diffusion limited. By direct coupling of H_2ase, or another redox active catalyst, to CdS as the absorber, with ligands that allow for near optimal orientations and fast ET, the upper limits of catalytic capacity can be explored. We expect that by addressing surface ligand limitations, nanocrystal−CaI biohybrids can sustain TOF's that approach the k_{cat} of CaI, illustrating the capacity of the extraordinary light-harvesting potential of nanocrystals, and fast catalytic rates of enzymes, for engineering direct photochemical solar energy conversion systems.

ASSOCIATED CONTENT

Supporting Information

Expression and purification protocol for ferredoxin, CdS nanorod synthesis, CdS nanorod potential determination, time-dependence of CdS:CaI self-assembly, Poisson distributions of CdS:CaI molar complexes for various CdS and CaI mixtures, effect of headspace H_2 on long-term CdS:CaI photocatalytic rates, QY measurement data, kinetic analysis of [AA] on photochemical H_2 production, CaI TOF dependence on CdS:CaI ratio and white light intensity, UV−vis absorption spectra during long-term H_2 generation, TEM images, and distributions of lengths and diameters at several time points. This material is available free of charge via the Internet at http://pubs.acs.org.

AUTHOR INFORMATION

Corresponding Author

Paul.king@nrel.gov; Gordana.dukovic@colorado.edu

Notes

The authors declare no competing financial interest.

ACKNOWLEDGMENTS

K.A.B. and P.W.K. gratefully acknowledge funding by the U.S. Department of Energy, Division of Chemical Sciences, Geosciences, and Biosciences, Office of Basic Energy Sciences. M.B. acknowledges support from the U.S. Department of Energy, Biological and Environmental Research Program for development of ferredoxin expression. K.A.B., M.B., and P.W.K also are grateful for the support by the U.S. Department of Energy under Contract No. DE-AC36-08-GO28308 with the National Renewable Energy Laboratory. M.B.W. and G.D. gratefully acknowledge support from University of Colorado Boulder startup funds and a seed grant from the Renewable and Sustainable Energy Institute (RASEI).

REFERENCES

(1) Balzani, V.; Credi, A.; Venturi, M. *ChemSusChem* **2008**, *1*, 26.
(2) Hambourger, M.; Moore, G. F.; Kramer, D. M.; Gust, D.; Moore, A. L.; Moore, T. A. *Chem. Soc. Rev.* **2009**, *38*, 25.
(3) Lewis, N. S.; Nocera, D. G. *Proc. Natl. Acad. Sci. U. S. A.* **2006**, *103*, 15729.
(4) Lubitz, W.; Reijerse, E. J.; Messinger, J. *Energy Environ. Sci.* **2008**, *1*, 15.
(5) Navarro, R.; Alvarez-Galvan, M.; de la Mano, J.; Al-Zahrani, S.; Fierro, J. *Energy Environ. Sci.* **2010**, *3*, 1865.
(6) Magnuson, A.; Anderlund, M.; Johansson, O.; Lindblad, P.; Lomoth, R.; Polivka, T.; Ott, S.; Stensjo, K.; Styring, S.; Sundstrom, V.; Hammarstrom, L. *Acc. Chem. Res.* **2009**, *42*, 1899.
(7) Arnon, D. I.; Losada, M.; Nozaki, M.; Tagawa, K. *Nature* **1961**, *190*, 601.
(8) Benemann, J. R.; Berenson, J. A.; Kaplan, N. O.; Kamen, M. D. *Proc. Natl. Acad. Sci. U. S. A.* **1973**, *70*, 2317.
(9) Ghirardi, M. L.; Posewitz, M. C.; Maness, P.-C.; Dubini, A.; Yu, J.; Seibert, M. *Annu. Rev. Plant Biol.* **2007**, *58*, 71.
(10) Hemschemeier, A.; Melis, A.; Happe, T. *Photosynth. Res.* **2009**, *102*, 523.
(11) McKinlay, J. B.; Harwood, C. S. *Curr. Opin. Biotechnol.* **2010**, *21*, 244.
(12) Rupprecht, J. *J. Biotechnol.* **2009**, *142*, 10.

(13) Gaffron, H.; Rubin, J. *J. Gen. Physiol.* **1942**, *26*, 219.
(14) Blankenship, R. E.; Tiede, D. M.; Barber, J.; Brudvig, G. W.; Fleming, G.; Ghirardi, M.; Gunner, M. R.; Junge, W.; Kramer, D. M.; Melis, A.; Moore, T. A.; Moser, C. C.; Nocera, D. G.; Nozik, A. J.; Ort, D. R.; Parson, W. W.; Prince, R. C.; Sayre, R. T. *Science* **2011**, *332*, 805.
(15) Grimme, R. A.; Lubner, C. E.; Bryant, D. A.; Golbeck, J. H. *J. Am. Chem. Soc.* **2008**, *130*, 6308.
(16) Utschig, L. M.; Dimitrijevic, N. M.; Poluektov, O. G.; Chemerisov, S. D.; Mulfort, K. L.; Tiede, D. M. *J. Phys. Chem. Lett.* **2011**, *2*, 236.
(17) Greenbaum, E. *Science* **1985**, *230*, 1373.
(18) Utschig, L. M.; Silver, S. C.; Mulfort, K. L.; Tiede, D. M. *J. Am. Chem. Soc.* **2011**, *133*, 16334.
(19) Ihara, M.; Nishihara, H.; Yoon, K.-S.; Lenz, O.; Friedrich, B.; Nakamoto, H.; Kojima, K.; Honma, D.; Kamachi, T.; Okura, I. *Photochem. Photobiol.* **2006**, *82*, 676.
(20) Lubner, C. E.; Grimme, R.; Bryant, D. A.; Golbeck, J. H. *Biochemistry* **2009**, *49*, 404.
(21) Brown, K. A.; Dayal, S.; Ai, X.; Rumbles, G.; King, P. W. *J. Am. Chem. Soc.* **2010**, *132*, 9672.
(22) Reisner, E.; Fontecilla-Camps, J. C.; Armstrong, F. A. *Chem. Commun.* **2009**, *5*, 550.
(23) Reisner, E.; Powell, D. J.; Cavazza, C.; Fontecilla-Camps, J. C.; Armstrong, F. A. *J. Am. Chem. Soc.* **2009**, *131*, 18457.
(24) Hambourger, M.; Gervaldo, M.; Svedruzic, D.; King, P. W.; Gust, D.; Ghirardi, M.; Moore, A. L.; Moore, T. A. *J. Am. Chem. Soc.* **2008**, *130*, 2015.
(25) Morra, S.; Valetti, F.; Sadeghi, S. J.; King, P. W.; Meyer, T.; Gilardi, G. *Chem. Commun.* **2011**, *47*, 10566.
(26) Bao, N.; Shen, L.; Takata, T.; Domen, K. *Chem. Mater.* **2007**, *20*, 110.
(27) Berben, L. A.; Peters, J. C. *Chem. Commun.* **2010**, *46*, 398.
(28) Helm, M. L.; Stewart, M. P.; Bullock, R. M.; DuBois, M. R.; DuBois, D. L. *Science* **2011**, *333*, 863.
(29) Sun, Y.; Bigi, J. P.; Piro, N. A.; Tang, M. L.; Long, J. R.; Chang, C. J. *J. Am. Chem. Soc.* **2011**, *133*, 9212.
(30) Acharya, K. P.; Khnayzer, R. S.; O'Connor, T.; Diederich, G.; Kirsanova, M.; Klinkova, A.; Roth, D.; Kinder, E.; Imboden, M.; Zamkov, M. *Nano Lett.* **2011**, *11*, 2919.
(31) Amirav, L.; Alivisatos, A. P. *J. Phys. Chem. Lett.* **2010**, *1*, 1051.
(32) Montini, T.; Gombac, V.; Sordelli, L.; Delgado, J. J.; Chen, X.; Adami, G.; Fornasiero, P. *ChemCatChem* **2011**, *3*, 574.
(33) Wen, F.; Yang, J.; Zong, X.; Ma, B.; Wang, D.; Li, C. *J. Catal.* **2011**, *281*, 318.
(34) Adams, M. W. W. *Biochim. Biophys. Acta* **1990**, *1020*, 115.
(35) Armstrong, F. A.; Belsey, N. A.; Cracknell, J. A.; Goldet, G.; Parkin, A.; Reisner, E.; Vincent, K. A.; Wait, A. F. *Chem. Soc. Rev.* **2009**, *38*, 36.
(36) Fauque, G.; Peck, H. D.; Moura, J. J. G.; Huynh, B. H.; Berlier, Y.; Dervartanian, D. V.; Teixeira, M.; Przybyla, A. E.; Lespinat, P. A.; Moura, I.; Legall, J. *FEMS Microbiol. Rev.* **1988**, *54*, 299.
(37) Fontecilla-Camps, J. C.; Amara, P.; Cavazza, C.; Nicolet, Y.; Volbeda, A. *Nature* **2009**, *460*, 814.
(38) Mulder, D. W.; Shepard, E. M.; Meuser, J. E.; Joshi, N.; King, P. W.; Posewitz, M. C.; Broderick, J. B.; Peters, J. W. *Structure* **2011**, *19*, 1038.
(39) Nicolet, Y.; Lemon, B. J.; Fontecilla-Camps, J. C.; Peters, J. W. *Trends Biochem. Sci.* **2000**, *25*, 138.
(40) Vignais, P. M.; Billoud, B. *Chem. Rev.* **2007**, *107*, 4206.
(41) Madden, C.; Vaughn, M. D.; Díez-Pérez, I.; Brown, K. A.; King, P. W.; Gust, D.; Moore, A. L.; Moore, T. A. *J. Am. Chem. Soc.* **2011**, *134*, 1577.
(42) Jones, A. K.; Sillery, E.; Albracht, S. P.; Armstrong, F. A. *Chem. Commun.* **2002**, 866.
(43) Pershad, H. R.; Duff, J. L.; Heering, H. A.; Duin, E. C.; Albracht, S. P.; Armstrong, F. A. *Biochemistry* **1999**, *38*, 8992.
(44) McDonald, T. J.; Svedruzic, D.; Kim, Y.-H.; Blackburn, J. L.; Zhang, S. B.; King, P. W.; Heben, M. J. *Nano Lett.* **2008**, *8*, 1783.
(45) Svedruzic, D.; Blackburn, J. L.; Tenent, R. C.; Rocha, J.-D. R.; Vinzant, T. B.; Heben, M. J.; King, P. W. *J. Am. Chem. Soc.* **2011**, *133*, 4299.
(46) Harris, L. A.; Wilson, R. H. *Annu. Rev. Mater. Sci.* **1978**, *8*, 99.
(47) Chen, X.; Shen, S.; Guo, L.; Mao, S. S. *Chem. Rev.* **2010**, *110*, 6503.
(48) Nozik, A. J. *Annu. Rev. Phys. Chem.* **1978**, *29*, 189.
(49) Berr, M.; Vaneski, A.; Susha, A. S.; Rodríguez-Fernández, J.; Döblinger, M.; Jäckel, F.; Rogach, A. L.; Feldmann, J. *Appl. Phys. Lett.* **2010**, *97*, 093108.
(50) Elmalem, E.; Saunders, A. E.; Costi, R.; Salant, A.; Banin, U. *Adv. Mater.* **2008**, *20*, 4312.
(51) Shemesh, Y.; Macdonald, J. E.; Menagen, G.; Banin, U. *Angew. Chem. Int. Ed.* **2011**, *50*, 1185.
(52) Aldana, J.; Lavelle, N.; Wang, Y. J.; Peng, X. G. *J. Am. Chem. Soc.* **2005**, *127*, 2496.
(53) Giz, M. J.; Duong, B.; Tao, N. J. *J. Electroanal. Chem.* **1999**, *465*, 72.
(54) King, P. W.; Posewitz, M. C.; Ghirardi, M. L.; Seibert, M. *J. Bacteriol.* **2006**, *188*, 2163.
(55) Demuez, M.; Cournac, L.; Guerrini, O.; Soucaille, P.; Girbal, L. *FEMS Microbiol. Lett.* **2007**, *275*, 113.
(56) Bradford, M. *Anal. Biochem.* **1976**, *72*, 248.
(57) Robinson, R. D.; Sadtler, B.; Demchenko, D. O.; Erdonmez, C. K.; Wang, L.-W.; Alivisatos, A. P. *Science* **2007**, *317*, 355.
(58) Dukovic, G.; Merkle, M. G.; Nelson, J. H.; Hughes, S. M.; Alivisatos, A. P. *Adv. Mater.* **2008**, *20*, 4306.
(59) Dimitrijevic, N. M.; Savic, D.; Micic, O. I.; Nozik, A. J. *J. Phys. Chem.* **1984**, *88*, 4278.
(60) Duonghong, D.; Ramsden, J.; Graetzel, M. *J. Am. Chem. Soc.* **1982**, *104*, 2977.
(61) Peters, J. W. *Curr. Opin. Struct. Biol.* **1999**, *9*, 670.
(62) Moulis, J.-M.; Davasse, V. *Biochemistry* **2002**, *34*, 16781.
(63) Dixon, M. *Biochem. J.* **1935**, *55*, 161.
(64) Dixon, M. *Biochem. J.* **1972**, *129*, 197.
(65) Segel, I. H. *Enzyme Kinetics: Behavior and Analysis of Rapid Equilibrium and Steady-State Enzyme Systems*; John Wilwy and Sons, Inc: New York, 1975.
(66) Chang, C. H.; King, P. W.; Ghirardi, M. L.; Kim, K. *Biophys. J.* **2007**, *93*, 3034.
(67) Natan, M. J.; Thackeray, J. W.; Wrighton, M. S. *J. Phys. Chem.* **1986**, *90*, 4089.
(68) Borsook, H.; Keighley, G. *Proc. Natl. Acad. Sci. U. S. A.* **1933**, *19*, 875.
(69) Aldana, J.; Wang, Y. A.; Peng, X. G. *J. Am. Chem. Soc.* **2001**, *123*, 8844.
(70) Alberty, R. A.; Hammes, G. G. *J. Phys. Chem.* **1958**, *62*, 154.
(71) Chou, K. C.; Zhou, G. P. *J. Am. Chem. Soc.* **1982**, *104*, 1409.
(72) Ghosh, S.; Bhattacharya, S.; Saha, A. *Anal. Bioanal. Chem.* **2010**, *397*, 1573.
(73) Wijffels, R. H.; Barbosa, M. J. *Science* **2010**, *329*, 796.
(74) Bielski, B. H. J.; Allen, A. O.; Schwarz, H. A. *J. Am. Chem. Soc.* **1981**, *103*, 3516.
(75) Bode, A. M.; Cunningham, L.; Rose, R. C. *Clin. Chem.* **1990**, *36*, 1807.
(76) Trotzky, S.; Kolny-Olesiak, J.; Falke, S. M.; Hoyer, T.; Lienau, C.; Tuszynski, W.; Parisi, J. *J. Phys. D: Appl. Phys.* **2008**, *41*, 102004.
(77) Beinert, H.; Holm, R. H.; Münck, E. *Science* **1997**, *277*, 653.
(78) Gillum, W. O.; Mortenson, L. E.; Chen, J. S.; Holm, R. H. *J. Am. Chem. Soc.* **1977**, *99*, 584.
(79) Vincent, K. A.; Belsey, N. A.; Lubitz, W.; Armstrong, F. A. *J. Am. Chem. Soc.* **2006**, *128*, 7448.
(80) Gillum, W. O.; Mortenson, L. E.; Chen, J. S.; Holm, R. H. *J. Am. Chem. Soc.* **1977**, *99*, 584.
(81) Lubner, C. E.; Applegate, A. M.; Knörzer, P.; Ganago, A.; Bryant, D. A.; Happe, T.; Golbeck, J. H. *Proc. Natl. Acad. Sci. U. S. A.* **2011**, *108*, 20988.
(82) Park, S. H.; Morgan, R. A.; Hu, Y. Z.; Lindberg, M.; Koch, S. W.; Peyghambarian, N. *J. Opt. Soc. Am. A* **1990**, *7*, 2097.

(83) Melis, A. *Plant Sci.* **2009**, *177*, 272.